Thermodynamics of fission products in $UO_{2 \pm x}$

2009 J. Phys.: Condens. Matter 21 435602

(http://iopscience.iop.org/0953-8984/21/43/435602)

J. Phys.: Condens. Matter **21** (2009) 435602 (9pp) doi:10.1088/0953-8984/21/43/435602

Thermodynamics of fission products in $UO_{2\pm x}$

P V Nerikar[1,2], X-Y Liu[2], B P Uberuaga[2], C R Stanek[2], S R Phillpot[1] and S B Sinnott[1]

[1] Department of Materials Science and Engineering, University of Florida, Gainesville, FL 32611, USA
[2] Materials Science and Technology Division, Los Alamos National Laboratory, Los Alamos, NM 87545, USA

E-mail: ssinn@mse.ufl.edu

Received 20 August 2009, in final form 14 September 2009
Published 8 October 2009
Online at stacks.iop.org/JPhysCM/21/435602

Abstract
The stabilities of selected fission products—Xe, Cs, and Sr—are investigated as a function of non-stoichiometry x in $UO_{2\pm x}$. In particular, density functional theory (DFT) is used to calculate the incorporation and solution energies of these fission products at the anion and cation vacancy sites, at the divacancy, and at the bound Schottky defect. In order to reproduce the correct insulating state of UO_2, the DFT calculations are performed using spin polarization and with the Hubbard U term. In general, higher charge defects are more soluble in the fuel matrix and the solubility of fission products increases as the hyperstoichiometry increases. The solubility of fission product oxides is also explored. Cs_2O is observed as a second stable phase and SrO is found to be soluble in the UO_2 matrix for all stoichiometries. These observations mirror experimentally observed phenomena.

1. Introduction

Fission products (FP) are produced during the burning of UO_2 [1]. Although the specific amount of a particular fission product generated depends on the composition of the fuel and the type of reactor, the general trends are similar. Since each FP has very different physical and chemical interactions with the fuel matrix, an assessment of its impact on the structural evolution of the fuel cannot be based on yield alone [2]. Some fission products do not react with the fuel matrix, some are as found as metallic precipitates, and others react with the fuel matrix to form separate phases. Therefore, in order to be able to predict the system behavior at a macroscopic level, it becomes very important to understand the behavior of fission products at the microscopic level.

Fission gases xenon (Xe) and krypton (Kr) are essentially insoluble in the UO_2 matrix and are present only by virtue of the fission process. Nevertheless, they can migrate to grain boundaries where they form bubbles. This bubble formation can lead to considerable swelling of the fuel and severely degrades mechanical properties [3]. These gases can also escape to the plenum region between fuel rod and the cladding, which can contribute to internal stresses on the cladding [4].

Solid-state fission products, such as cesium (Cs), can assume various roles depending on conditions prevailing in the matrix. They are found as a minor component of the gray phase, which is a separate phase consisting of a number of fission products [5, 6]. Cs in particular is found as a metallic inclusion in the fuel, though implantation studies have observed it to be present on lattice sites in hyperstoichiometric fuels [7]. It can also react with iodine (I) and cause corrosion of cladding materials such as zircaloy and stainless steel [8]. The fission product strontium (Sr) is generally considered to be soluble in UO_2 [6, 9], although the extent of solubility critically depends on the oxygen to metal ratio. In the presence of another fission product zirconium (Zr), it tends to form a gray phase perovskite $SrZrO_3$ [10].

There is a significant need for an in-depth analysis of the interaction of fission products with the various defects present in UO_2 from reliable calculations and simulations. Grimes and Catlow [11] presented a comprehensive study of the variety of fission products formed and developed a theoretical model that provides atomic level explanations to experimentally observed phenomena. In particular, they used the Mott–Littleton [11, 12] approach and empirical potentials to calculate all the relevant energies. However, their work used fixed charge empirical

potentials to calculate defect energies, which neglect charge transfer effects that may be important in some situations. Petit and co-workers [13–16] performed similar calculations using DFT. They used the local density approximation (LDA) and the generalized gradient approximation (GGA). However, their calculations were limited to 24-atom supercells. Moreover, it has been shown [17–19] that the localization of the 5f orbital of uranium plays a dominant role in determining the correct electronic structure of UO_2 and consequently on the defect formation energies, which conventional LDA and GGA fail to capture; this effect can be captured using the Hubbard $+U$ on-site repulsion. More recently, Brillant *et al* [20] used the spin polarized SP-GGA $+ U$ method and a 96-atom supercell to calculate the incorporation and solution energies of barium (Ba) and zirconium (Zr) and their respective oxides in $UO_{2\pm x}$. It was found that the most stable incorporation site for the fission product depended on the type of DFT functional used and the effects of functional form were more pronounced for higher charged defects. A very recent paper by Gupta *et al* [21] discusses solution and migration of cesium in UO_2. They observed the solution of cesium to be very low and the migration to be highly anisotropic.

In this work, we use SP-GGA $+ U$ and non-spin polarized GGA method to analyze the incorporation and solubility of Xe, Cs, and Sr in the UO_2 matrix. These fission products have been selected due to their very different characteristics and interactions with the fuel matrix. In contrast to GGA, the SP-GGA $+ U$ method correctly predicts the experimentally observed insulating behavior of UO_2 [22].

Our DFT calculations are supported by empirical potential calculations to test the interaction of periodic images. This becomes important when considering large-sized fission products and extended defects such as the bound Schottky defect. Finally, we have also used our SP-GGA $+ U$ results in a point defect model that can predict the change in formation energies of point defects with variations in temperature and stoichiometry.

The rest of this paper is organized as follows: section 2 discusses the computational methods used, including the details of how the different energies associated with the inclusion of fission products are determined. The results of the SP-GGA $+ U$ calculations are discussed in section 3, beginning with the validation of the adopted approach by considering equilibrium properties such as lattice parameter and the defect formation energies of neutral defect complexes in UO_2 (section 3.1). Next, the incorporation energies of fission products are compared with the findings of previous theoretical studies (section 3.2). Since the solution energies can be directly correlated to experimentally observed phenomena, they are considered next (section 3.3). The effect of oxide solution energies is discussed in section 3.4. The comparison of SP-GGA $+ U$ results with our GGA and previously published empirical potential results is carried out in section 4. Section 5 gives the conclusions of this work.

Table 1. Comparison of equilibrium and defect properties of UO_2 from GGA, SP-GGA $+ U$ and experiment.

Method	Lattice parameter (Å)	Anti-Frenkel (eV)	Frenkel (eV)	Schottky (eV)
Experiment	5.47 [29]	3.0–4.6 [29]	8.5–9.6 [29]	6.0–7.0 [29]
GGA	5.35	3.77	9.09	5.02
SP-GGA $+ U$	5.49	3.95	15.08	7.6

2. Computational methodology

2.1. Electronic structure calculations

The DFT calculations were performed with the projector augmented-wave (PAW) [23, 24] method. We utilized the SP-GGA $+ U$ [25] to include the effect of the strong correlation of 5f electrons in uranium and non-spin-polarized GGA as implemented in the Vienna *ab initio* simulation package (VASP) [26, 27]. We use a U_{eff} $(U - J)$ value of 3.96 eV for our SP-GGA $+ U$ calculations. This value is similar to those previously used by others [17, 18, 25] and also to experimental measurements [22]. With regard to other calculation parameters, we used a $2 \times 2 \times 2$ unit cell for the structural optimizations where the cell volume was kept constant and the atomic positions relaxed. The Brillouin zone sampling used a $2 \times 2 \times 2$ Monkhorst–Pack k-point mesh [28]; the cut-off energy for the plane waves was 400 eV. We used a strict force and energy convergence criteria for these calculations (see [19] for details). The combination of the above parameters resulted in good agreement with experiments for bulk and defect properties (see table 1). All the fission products considered are charge neutral.

2.2. Incorporation energy

The incorporation energy is the energy required to take a fission product from infinity and place it at a pre-existing trap site. The incorporation energy of a fission product is defined by Grimes *et al* [11] as:

$$E_{\text{inc.}} = E^{\text{total}}(\alpha) - E^{\text{total}}(\text{defect}) - E_i. \tag{1}$$

Here $E^{\text{total}}(\alpha)$ is the total energy of the cell with the fission product at a particular defect site, $E^{\text{total}}(\text{defect})$ is the total energy of the cell with a particular defect, and E_i is the energy of a single isolated fission product. This energy does not account for the formation of the trap site and assumes that there is always an excess of available sites. This assumption is only valid at low burn-ups, i.e., when the concentration of fission products is low. This definition also does not account for changes in fuel stoichiometry. Nevertheless, it is a useful quantity that measures the energetics of fission products at different trap sites. A positive value of the incorporation energy means that energy is required to place a fission product at a particular trap site. In this work, the trap sites we have considered are the empty octahedral interstitial site, oxygen vacancy, uranium vacancy, a neutral divacancy (consisting of a uranium and oxygen vacancy in close proximity) and finally a

neutral trivacancy (bound Schottky defect). The configuration of the Schottky defect used here is the same as that used by Grimes *et al* [11].

2.3. Solution energy

To compensate for limitations of incorporation energy, we also consider the solution energy of fission products. The solution energy is defined as [11]

$$E_{\text{solution}} = E_{\text{inc.}} + E_{\text{trap}} \tag{2}$$

where E_{trap} is the trap site formation energy, which is defined as the energy required to form a particular trap site for the incorporation of a fission product. Thus, the solution energy accounts for both the formation of the trap site as well as the incorporation of the fission product into that trap site. This energy will be a function of stoichiometry and hence burn-up. For example, it will be harder to form an oxygen vacancy in a hyperstoichiometric case (UO_{2+x}) compared to a hypostoichiometric case (UO_{2-x}). One advantage of the solution energy compared to the incorporation energy is that it can be correlated to experimental trends. As with the incorporation energy, this definition assumes no interaction, such as clustering, between fission products.

Experimentally, the concentration of fission products is determined by the fission reactions, whereas computationally the fission products are introduced manually. To evaluate the trap site formation energy as a function of stoichiometry, we have implemented a point defect model (PDM). This model helps relate the experimental and computational findings to one another. Using such a model, the apparent trap site formation energy can be calculated, effectively taking into account several defect formation reactions at once. As the relative importance of different reactions will change with temperature and stoichiometry, the effect of temperature and stoichiometry on the formation energy can also be determined. The apparent trap site formation energy is obtained through

$$E_{\text{trap}} = -kT \ln([X]) \tag{3}$$

where $[X]$ is the concentration of the type of defect X considered. As discussed by Crocombette *et al* [13] the evaluation of the apparent defect formation energies can be expressed in the framework of a PDM, originally introduced by Matzke [29] and Lidiard [30]. In the PDM, the concentrations of point defects in $UO_{2\pm x}$ are governed by of the kinetic equations:

$$[\mathrm{V_O}][\mathrm{I_O}] = \exp\left(-\frac{E^{\mathrm{F}}_{\mathrm{FP_O}}}{kT}\right), \tag{4}$$

$$[\mathrm{V_U}][\mathrm{I_U}] = \exp\left(-\frac{E^{\mathrm{F}}_{\mathrm{FP_U}}}{kT}\right), \tag{5}$$

$$[\mathrm{V_O}]^2[\mathrm{V_U}] = \exp\left(-\frac{E^{\mathrm{F}}_{\mathrm{S}}}{kT}\right), \tag{6}$$

$$2[\mathrm{V_U}] + [\mathrm{I_O}] = 2[\mathrm{I_U}] + 2[\mathrm{V_O}] + x. \tag{7}$$

Here $[\mathrm{V_O}]$, $[\mathrm{I_O}]$, $[\mathrm{V_U}]$ and $[\mathrm{I_U}]$ are the concentrations of the oxygen vacancy, oxygen interstitial, uranium vacancy and uranium interstitial respectively; $E^{\mathrm{F}}_{\mathrm{FPO}}$, $E^{\mathrm{F}}_{\mathrm{FPU}}$ and $E^{\mathrm{F}}_{\mathrm{S}}$ are the formation energies of the anti-Frenkel, Frenkel and Schottky complexes. In addition, the concentrations of divacancy and bound Schottky defects are given by

$$[\mathrm{DV}] = [\mathrm{V_O}][\mathrm{V_U}] \exp\left(-\frac{B_{\mathrm{DV}}}{kT}\right), \tag{8}$$

$$[\mathrm{Sch}] = [\mathrm{V_O}]^2[\mathrm{V_U}] \exp\left(-\frac{B_{\mathrm{Sch}}}{kT}\right). \tag{9}$$

Here, B_{DV} and B_{Sch} are the binding energies of divacancy and Schottky defects. The binding energies were calculated by taking the difference of formation energies when the defects were separated and when they were in close proximity. The numerical values are 3.67 eV and 5.1 eV for the divacancy and Schottky defects, respectively.

To solve equations (4)–(7), we make the assumption that the uranium interstitial concentration is negligible compared to other defect concentrations, an assumption that we shall see leads to a consistent solution to the equations. With this assumption, equations (4)–(7) lead to a cubic equation for $[\mathrm{V_O}]$ or $[\mathrm{I_O}]$. By solving the cubic equations using standard techniques with complex solutions, the concentration of oxygen vacancies or oxygen interstitials and, in turn, their formation energies as a function of stoichiometry are obtained. The concentrations of other defects are then determined with equations (4)–(9). In the PDM, the inputs are the formation energies of defect complexes, determined from first principles, and the concentrations of individual point defects are then calculated. The resulting apparent formation energies we find agree well with experimentally observed trends in that the oxygen Frenkel pair is predicted to be the most stable defect complex. This relative stability does not change with the exchange correlation functional used, although the absolute values may be different as pointed out by Geng *et al* through their LSDA + U calculations.

2.4. Oxide solution energy

Solid fission products such as cesium and strontium can react with oxygen in the fuel, and form secondary oxide phases [1]. Any oxide (for example, strontium oxide) before solution into the UO_2 matrix will decompose into the fission product and oxygen by the following reaction:

$$\mathrm{SrO(s)} \longrightarrow \mathrm{Sr} + \mathrm{O(g)}. \tag{10}$$

Thus, although the calculation of the solution energy is useful in predicting the most stable trap site as a function of stoichiometry, its definition is limited to isolated fission products. For example, it does not provide information about whether the fission product would remain in the UO_2 matrix or whether it would react with oxygen to form a stable second phase. Therefore, a third definition of energy is required; the fission product oxide solution energy is given as

$$E^{\text{solution}}_{\mathrm{SrO}} = E^{\text{solution}}_{\mathrm{Sr}} + E^{\text{solution}}_{\mathrm{O}} - E^{\text{formation}}_{\mathrm{SrO}}. \tag{11}$$

The first term on the right-hand side of the equation is the solution energy of the particular fission product at the most

stable trap site based on stoichiometry; the second term is the solution energy of the oxygen from the fission product oxide into any vacant oxygen site in the UO_2 matrix. This vacant site also depends on stoichiometry. In UO_{2-x}, the oxygen will be soluble in an oxygen vacancy site, while in UO_{2+x} it will be present as an oxygen interstitial site, and in UO_2 the most stable solution site will be a mixture of vacancy and interstitial sites. We have calculated the solution energy of all possible oxygen solution sites and observed that oxygen has the lowest solution energy in the interstitial site in UO_{2+x}.

Geng *et al* [31] showed that above $UO_{2.03}$, oxygen clustering is inevitable. However, the objective of the present work is to observe the effect of stoichiometry as predicted by the PDM, which is valid for stoichiometries of $x < 0.03$. It is also important to note that the even though clustering is inevitable, the actual mechanism of clustering is not well understood. For example, Geng *et al* [32, 33] showed that a cuboctahedral cluster is the most stable while Andersson *et al* [34] determined that 4-atom clusters (the so-called split quadinterstitial structure) to be more favorable. Hence, further work is clearly required before assuming a given defect cluster as a reference state.

The third term in equation (11) is the formation energy of the oxide. Both SrO and Cs_2O were considered in their standard crystalline states. The energies of the oxides were calculated with respect to an oxygen molecule reference state in order to maintain a consistent reference state across the various systems under consideration. The formation energies of binary oxides were calculated using conventional GGA, which is known to appropriately describe delocalized orbitals. If the fission product oxide solution energy is negative, it means that it is energetically favorable for the oxide to be soluble in the fuel. This in turn means that the fission product will not form a stable second phase. This definition neglects contributions from interfacial energy that would be required to create a stable second phase.

3. Results and discussion

3.1. Validation of approach

The first step in validating our approach is to calculate equilibrium and defect properties for UO_2. Table 1 summarizes the earlier [19] comparison of the lattice parameter and formation energies of defect complexes in UO_2 calculated using SP-GGA + U and GGA with published experimental results. We find that the agreement with experiment improves if SP-GGA + U is used. As expected, the GGA method underestimates the lattice parameter of UO_2 slightly. The calculated defect energies using SP-GGA + U are in good agreement with experiment for the case of the anti-Frenkel defect and agree reasonably well for the unbound Schottky defect as compared to experimental data. However, the SP-GGA + U method predicts a higher Frenkel formation energy than experiment. This value has been suggested to be an underestimate in experimental results [35] as discussed previously [19]. Regardless of whether it is an underestimate or not, the Frenkel defect has very high formation energy and is ignored in our further calculations. The differences in the defect energies between different SP-GGA + U calculations arise due the distributions of magnetic moments of the U^{5+} ions, as discussed in section 3.2. Additionally, Geng *et al* [31] concluded that it is the U parameter, and not the exchange–correlation functional (GGA), that is important when we approach hyperstoichiometric conditions. In any case, we have calculated the concentrations of different oxygen defects using the PDM in UO_{2+x} found that the interstitial is the majority defect. The focus of the DFT results will be on the SP-GGA + U results, and in section 4.1, a further comparison to GGA will be made.

Our DFT calculations are all performed in a $2 \times 2 \times 2$ supercell size with 96 atoms under constant volume conditions. The consideration of limitations of system size is important, as there could be interactions between periodic images of the defect in neighboring supercells, especially for the case where a fission product is placed in a vacant site or the cell is not charge neutral. Because of the computational expense, the system sizes that can be treated with DFT are necessarily small. It is also known that for increasingly larger system sizes, the differences between the constant volume and constant pressure become smaller. To estimate the effects of the limited supercell size used and the constant volume constraint, we performed fission product incorporation calculations using an empirical potential within the general utility lattice program (GULP) [36, 37]. The advantage of this approach is that larger supercell sizes can be treated with negligible computational cost. Because of the intrinsic limitations of empirical potential approaches, these values can be expected to be less accurate than those obtained with DFT. However, the effects of supercell size, which arise primarily from electrostatic and elastic interactions, are not expected to change significantly with method [19]. We have chosen the Grimes potential [11] for these GULP calculations, which has the advantage of being parameterized for a variety of fission product interactions with the UO_2 host. We have analyzed the effect of system size for Cs incorporation (figure 1) into the empty octahedral interstitial site, oxygen vacancy site, and uranium vacancy site.

As expected, we find that the incorporation energy converges as the system size increases. For the octahedral and the oxygen vacancy sites, the energy is nearly converged at a system size of $2 \times 2 \times 2$. For the uranium vacancy site, the energy changes by about 16% as the system size is increased from $2 \times 2 \times 2$ to $3 \times 3 \times 3$. This kind of analysis gives us confidence that there are no strong interactions between neighboring periodic images and the supercell considered in the DFT calculations is sufficiently large. More importantly, the physical trends are similar for the system sizes considered, which is the objective of the current work.

The third step in our approach is to validate the point defect model that we have implemented. Grimes and Catlow [11] developed a series of equations (hereafter referred to as the Grimes model) to calculate the trap site formation energy (E_{trap}) based on the anti-Frenkel and Schottky defect formation energies. This model provides a convenient way of estimating the solution energy of fission products as a function of stoichiometry. However, since it considers only the most

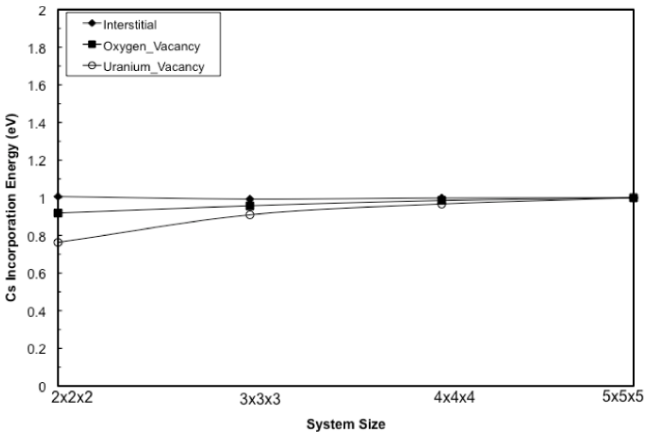

Figure 1. Normalized incorporation energy of cesium in pre-existing trap sites calculated as function of system size by atomic level simulations using an empirical potential within GULP. The system sizes are multiples of the conventional fluorite cell along the x, y and z directions. The energies have been normalized with respect to the $5 \times 5 \times 5$ system.

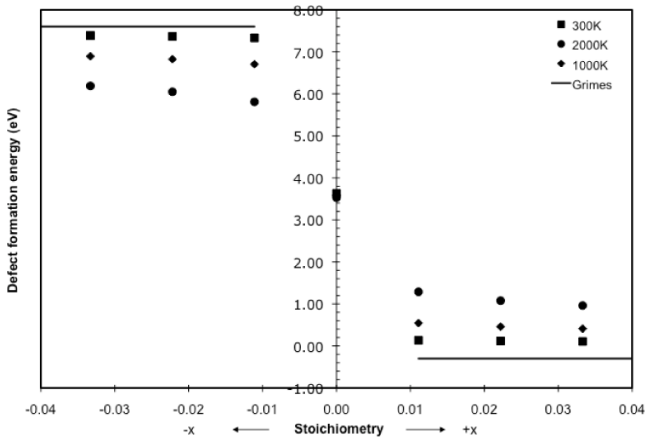

Figure 2. Formation energy of a uranium vacancy calculated using SP-GGA + U method as a function of temperature and stoichiometry using the point defect model. The temperatures taken into account are 300, 1000 and 2000 K. The flat lines on the plot are the uranium vacancy formation energy values as calculated using the Grimes model.

dominant reaction for the formation of a given trap site, it does not account for temperature variations. The approach we have adopted (equations (4)–(9)) compares the trap site formation energy (E_{trap}) calculated using both the Grimes model and the PDM and analyzes the scenarios by which these simplified expressions are valid to determine when a more complex assessment is required.

The formation energy of a uranium vacancy is plotted as a function of stoichiometry in figure 2 at 300, 1000 and 2000 K. The stoichiometry is varied from $UO_{1.97}$ to $UO_{2.03}$. The temperature effect is included through the PDM described by equations (4)–(9), while the results using the Grimes model correspond to 0 K. The inputs (defect formation energies) for both models are from SP-GGA + U calculations. The results of the DFT calculations confirm the conclusion of the Grimes model on the low-temperature defect formation reactions, where there is good agreement. The agreement gets worse as the temperature is increased. The reason for this trend is that at lower temperatures only the anti-Frenkel mechanism is dominant, which is similar to the prediction of the Grimes model. However, as the temperature increases, other mechanisms such as the Schottky defect formation become important. Thus, at lower temperatures, it is valid to use the Grimes model to calculate the trap site formation energy, but at higher temperatures, such as those found in a light water reactor, more complicated expressions have to be considered. This effect is even more pronounced when the deviations from stoichiometry are small.

3.2. Incorporation energy

The incorporation energies of Xe, Cs and Sr calculated using DFT are reported in table 2. The lowest value for each fission product is shown in bold. First considering the inert fission gas (Xe), the bound Schottky defect is predicted to be the most stable incorporation site. Moreover, the trend can be related to the relative size of the incorporation sites. The bound Schottky defect is the largest of the defects considered here, even though it has high formation energy. However, the incorporation energy, by definition, does not account for the formation of the defect.

Table 2. Incorporation energies of xenon, cesium and strontium calculated using SP-GGA + U and GGA and compared to previous empirical potential results. For each of the fission product, the lowest incorporation energy is shown in bold.

	SP-GGA + U	GGA	Grimes
	Xe		
Interstitial	11.11	12.75	17.23
O vacancy	9.5	9.71	13.34
U vacancy	2.5	6.04	4.99
Divacancy	2.45	3.29	2.84
Schottky	**1.38**	**2.12**	**1.16**
	Cs		
Interstitial	10	10.1	9.93
O vacancy	8.4	8.1	9.1
U vacancy	**−3.4**	0.75	**−6.08**
Divacancy	−1.99	0.23	−5.63
Schottky	−0.8	**−0.38**	−5.47
	Sr		
Interstitial	4.68	4.3	−11.04
O vacancy	7.18	5.3	−8.87
U vacancy	**−9.66**	**−5.4**	**−27.09**
Divacancy	−7.53	−4.97	−25.31
Schottky	−4.55	−4.74	−23.36

The SP-GGA + U method predicts the uranium vacancy to be the most stable incorporation site for cesium. This can be understood by considering Coulombic effects. The Cs^{+} ion would prefer to reside on a uranium vacancy (U^{4+}) since the Coulombic forces are stronger. The trend is in agreement with the calculations of Gupta *et al* [21]. However, our incorporation energy values are higher even though the calculation method is similar. This can be attributed to the

differences in ordering of magnetic moments of the uranium ions. It is well known from published literature [34, 38, 39] that in the SP-GGA + U scheme, multiple minima exist and it is almost impossible to find the 'true' ground state. The total energy depends on the starting point of the calculation and also on the distribution of U^{5+} ions. Therefore, it is normal to obtain different absolute energies. It is important to note, however, that we do not expect the physical properties to change with different states. For similar reasons of Coulombic interactions, the uranium vacancy is predicted to be the most stable incorporation site for a Sr^{2+} ion.

3.3. Solution energy

The calculated solution energies are presented in table 3; for each stoichiometry, the lowest solution energy is shown in bold. The results in table 3 are also illustrated in figure 3. Here Sr_int., Sr_O and Sr_U refer to a Sr atom on an empty interstitial site, an oxygen vacancy and an uranium vacancy respectively. The apparent trap site formation energy values used are those found with the PDM at 300 K. The results can be understood based on the relationship between the incorporation energy and the apparent formation energy of a particular defect as a function of stoichiometry. The first point to notice is that the solution energy of xenon is independent of stoichiometry for the interstitial and the bound Schottky site. The interstitial site is empty and therefore no defects have to be created to incorporate xenon into that site. The definition for the apparent formation of the Schottky site is the energy difference between the actual Schottky formation energy (when the constituent defects are far apart) and the binding energy of the neutral trivacancy (when the defects are in close proximity). For UO_{2-x}, the bound Schottky site is predicted to be the most stable solution site. This is true even though it is easier to form an oxygen vacancy than a bound Schottky defect, since the incorporation of xenon in the latter is energetically favorable compared to the former. This is due to the larger size of the bound Schottky defect.

In UO_2, the divacancy formation energy is less than that of bound Schottky defect since it is more difficult to form oxygen vacancies in UO_2 compared to UO_{2-x}. Hence there is a competition between the most stable solution sites. It becomes even more difficult to form oxygen vacancies and easier to form uranium vacancies in UO_{2+x}. Hence, xenon is predicted to occupy the single cation site. As previously mentioned, solution energy results can be correlated directly with experimental trends. The calculated solution energy of xenon is positive and high for all stoichiometries. Therefore, it is insoluble in the UO_2 matrix in accordance with experimental findings [3] and is only found as a consequence of the fission process.

The results for fission gases can be understood as a balance between the size of the trap and the energy to form the trap. However, for solid fission products such as cesium and strontium, the effect of charge must also be taken into account. In UO_{2+x}, the uranium vacancy has the lowest formation energy and hence solution of cesium is favored at this site. In UO_2, the divacancy has a larger size and slightly overcomes

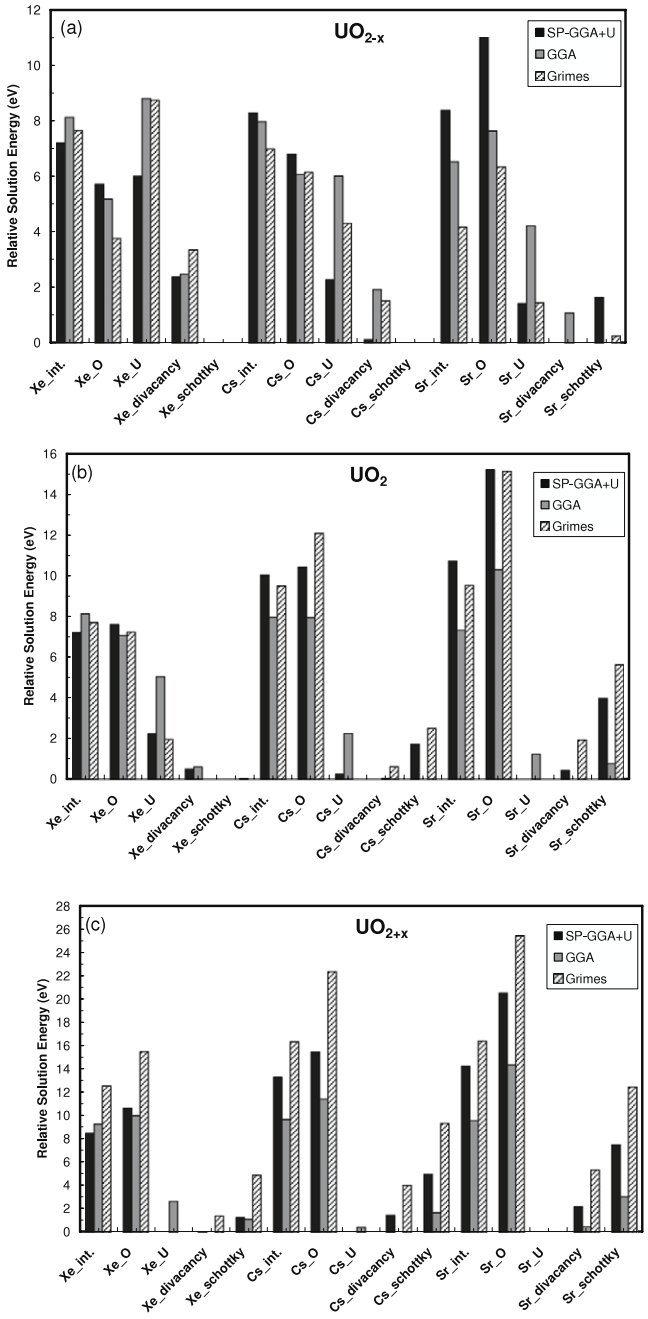

Figure 3. Solution energies of Xe, Cs and Sr in UO_2 relative to the lowest solution energy site for a particular stoichiometry (a) UO_{2-x}, (b) UO_2, (c) UO_{2+x}.

the more highly charged uranium vacancy as the most stable solution site even though both have similar formation energies. In hypostoichiometric conditions, due to the availability of oxygen vacancies the most stable site is the bound Schottky defect. In agreement with an implantation study by Matzke [7], our calculations predict that cesium will occupy a lattice site (uranium vacancy in this case) in hyperstoichiometric fuels.

The divacancy trap site is favored for the solution of strontium in sub-stoichiometric (UO_{2-x}) environments relative to the bound Schottky defect. However, as the matrix becomes hyperstoichiometric, the formation energy of a uranium

Table 3. Solution energies of xenon, cesium and strontium calculated using SP-GGA + U and GGA and compared to previous empirical potential results. For each of the fission product and stoichiometry, the lowest solution energy is shown in bold.

	SP-GGA + U			GGA			Grimes		
Trap Site	UO_{2-x} ($UO_{1.97}$)	$UO_{2.00}$	UO_{2+x} ($UO_{2.03}$)	UO_{2-x} ($UO_{1.97}$)	UO_2	UO_{2+x} ($UO_{2.00}$)	UO_{2-x}	UO_2	UO_{2+x}
				Xe					
Interstitial	11.10	11.10	11.10	12.75	12.75	12.75	17.23	17.23	17.23
O vacancy	9.61	11.48	13.25	9.82	11.69	13.46	13.34	16.75	20.16
U vacancy	9.89	6.13	**2.61**	13.43	9.67	6.15	18.32	11.50	**4.68**
Divacancy	6.27	4.40	2.63	7.11	5.24	**3.47**	12.93	**9.52**	6.11
Schottky	**3.88**	**3.88**	3.88	**4.62**	**4.62**	4.62	**9.57**	**9.57**	9.57
				Cs					
Interstitial	10.00	10.00	10.00	10.10	10.10	10.10	9.93	9.93	9.93
O vacancy	8.51	10.38	12.15	8.21	10.08	11.85	9.10	12.50	15.92
U vacancy	3.99	0.23	**−3.29**	8.14	4.38	0.86	7.26	**0.43**	**−6.39**
Divacancy	1.83	**−0.04**	−1.81	4.05	**2.18**	**0.41**	4.47	1.06	−2.35
Schottky	**1.70**	1.70	1.70	**2.12**	**2.12**	2.12	**2.94**	2.94	2.94
				Sr					
Interstitial	4.68	4.68	4.68	4.30	4.30	4.30	−11.04	−11.04	−11.04
O vacancy	7.29	9.16	10.93	5.41	7.28	9.05	−8.87	−5.46	−2.05
U vacancy	−2.27	**−6.03**	**−9.55**	1.99	−1.77	**−5.29**	−13.76	**−20.58**	**−27.41**
Divacancy	**−3.71**	−5.58	−7.35	−1.15	**−3.02**	−4.79	**−15.22**	−18.63	−22.04
Schottky	−2.05	−2.05	−2.05	**−2.24**	−2.24	−2.24	−14.95	−14.95	−14.95

vacancy drops significantly and it becomes the dominant solution site for UO_{2+x}. A similar trend has been observed for barium by Brilliant *et al* [20]. This is expected as both elements belong to the same group in the periodic table and the calculation techniques are quite similar. Strontium solubility increases in the hyperstoichiometric regime as observed experimentally [9].

It must be noted, however, that the solution energies have been calculated at 300 K and the most stable site can change with temperature. This is observed for the case of Cs solution in the hypostoichiometric case where the solution site changes from the Schottky site to the divacancy site with increase in temperature. This can have important ramifications on the prediction of fuel behavior as different parts of the fuel are at different temperatures.

3.4. Oxide solution energy

The oxygen solution energies are reported in table 4. A positive value corresponds to the oxide being insoluble in the fuel and forming a second stable phase. We find that oxides with higher oxygen-to-metal ratio are more soluble in the fuel. This can be understood on the basis of their ability to donate oxygen to the lattice. The solubility also increases as the hyperstoichiometry of the UO_2 increases. Considering individual oxides, Cs_2O is predicted to be stable at all stoichiometries, though in UO_{2+x}, it has borderline stability. With regard to UO_{2+x}, it is observed experimentally [6] that the solubility of Cs increases as we go from hypostoichiometric to hyperstoichiometric fuels, in agreement with our calculations. This can again be related to the argument that the more oxygen an oxide donates to the fuel matrix, the more soluble it is [11].

The maximum solubility of SrO in UO_2 was estimated to be 12 mol% at 1773 K by Kleykamp *et al* [9] and the solubility has to decrease with decreasing temperature as some degree of that solubility has to be driven by entropy. However, our calculations predict SrO to be soluble in UO_2 for all the three stoichiometries at the dilute limit. If no Sr–Sr interaction is assumed, this implies complete solubility of Sr, which is clearly at odds with the experimental result. To resolve this contradiction, we performed calculations where two Sr atoms are placed 3.88 Å apart (the closest cation–cation distance in a fluorite structure) in the same supercell. The calculated interaction energy is 1.35 eV, which suggests strong Sr–Sr repulsion and is of the same order of magnitude as the oxide solution energy. This result strongly suggests that there is a limit to the solubility of Sr in UO_2. Our results in table 4, valid only for a dilute limit of strontium, predict Sr is soluble at the 3 mol% level. However, as more Sr is added, the Sr ions would begin to repel, and the solubility would peak. Assuming that this repulsion is only for nearest-neighbor Sr ions, this would predict a maximum solubility of 25%, which clearly indicates that the repulsion is even longer ranged. Our calculations neglect entropic contributions but take charge transfer into account (four U^{5+} species to compensate for the two strontium

Table 4. Solution energies of oxides of cesium and strontium calculated using SP-GGA + U and GGA and compared to previous empirical potential results. A positive energy implies insolubility in the fuel matrix phase.

	SP-GGA + U			Grimes		
Oxide	UO_{2-x} ($UO_{1.97}$)	UO_2	UO_{2+x} ($UO_{2.03}$)	UO_{2-x}	UO_2	UO_{2+x}
SrO	−0.85	−1.3	−3.04	2.43	0.48	−2.93
Cs_2O	2.10	2.23	0.76	10.58	8.98	−1.25

atoms; these species are separated by at least 6 Å to minimize repulsion).

In addition, the solubility of Sr was observed to be much higher in UO_2 than in UO_{2-x} by Kleykamp *et al*, which mirrors our calculated trend. This can be explained by the fact that the solution of strontium becomes increasingly favorable as one approaches hyperstoichiometric conditions owing to the strong Coulombic interactions. The higher charged uranium vacancy (4+) is the most stable solution site in UO_2 as compared to the divacancy (2+) site in UO_{2-x} and hence has a strong preference for charged cations. Our calculations agree well with BaO solubility calculations of Brillant *et al* [20] and experimental observations of Thomas *et al* [40], in which they found that barium does not precipitate in low burn-up hypostoichiometric fuels and mid burn-up hyperstoichiometric fuels. This is again expected since barium and strontium are quite similar in their chemical and physical make-up.

4. Comparison with other theoretical approaches

Theoretical progress has led, and continues to lead, to DFT formalisms of ever increasing materials fidelity. It is thus valuable to assess the applicability of various formalisms to our problem. Thus, in this section the results from GGA and SP-GGA + U are compared. The results of the DFT calculations are also compared with the results obtained with empirical potentials.

4.1. Non-spin polarized GGA

The incorporation energies of Xe, Cs and Sr calculated using GGA are reported in table 2 and compared with the SP-GGA + U results. When considering the incorporation of Xe, there is qualitative and quantitative agreement between both approaches. Both methods predict the bound Schottky site to be the most stable. This is not unexpected, as the stability of this particular fission product is a direct result of the relative sizes of the incorporation sites.

When considering the incorporation of cesium, there is a discrepancy between SP-GGA + U and GGA. GGA predicts the most stable site to be the bound Schottky defect while SP-GGA + U predicts it to be the uranium vacancy site. Since GGA does not predict an ionic or insulating ground state for UO_2, it only partially captures the relevant Coulombic effects. These effects become even stronger for Sr and hence both methods predict the uranium vacancy to the most stable site, although the stability of this site with GGA is only marginal.

The solution energies of these defects are reported in table 3 as a function of stoichiometry and the most stable site is again shown in bold. For Xe, GGA and SP-GGA + U predict the bound Schottky to be the most stable solution site for UO_{2-x} and UO_2. However, for UO_{2+x}, GGA predicts the divacancy site to be energetically favorable in contrast to SP-GGA + U, which predicts the uranium vacancy site to be the most stable. As discussed previously, the solution energy is a balance of the incorporation and apparent formation energies. There is a significant difference in the incorporation energy of Xe at the uranium vacancy site between the two methods and this becomes dominant in the hyperstoichiometric case.

For Cs, GGA does not predict any solubility for any stoichiometry owing to the incorrect treatment of the Coulombic effects, as opposed to SP-GGA + U that finds Cs to be soluble in UO_2 and UO_{2+x}. For Sr, there is qualitative agreement between the two methods in that the solubility of Sr increases as the matrix becomes hyperstoichiometric. However, the repulsion predicted by GGA for two strontium atoms in the same supercell is negligible (∼0.1 eV compared to 1.35 eV with GGA + U) and thus cannot explain the contradiction between experiment and the calculated results.

Thus, in general, we find that the non-spin polarized GGA results agreed with the SP-GGA + U results when the Coulombic interactions are absent, as in the case of Xe, or when they are present and strong (Sr).

4.2. Empirical potentials

The incorporation energies for Xe, Cs and Sr from reported empirical potential calculations [11] are also compared with our SP-GGA + U results in table 2. There is an overall qualitative agreement in trends between the two methods. However, the absolute values of incorporation energies predicted by empirical potentials are significantly higher, especially for higher charged ions. A probable cause for this could be the use of formal charges in the empirical potentials, which tends to lead to overestimations of binding energies [35].

With regard to the solution energies (table 3), the trends are similar for both methods for all stoichiometries. Both methods predict that the solution of all the three fission products considered becomes energetically favorable as the matrix becomes hyperstoichiometric. In particular, they agree on the most stable solution sites except for Cs in the stoichiometric case.

4.3. Published DFT work

The incorporation and solution energies of Kr, Cs and Sr have been calculated previously [13] using LDA formalism and can be qualitatively compared to our results. These calculations were done on a 24-atom supercell. Hence, they did not consider the divacancy and the bound Schottky trap sites, which have been shown in this work to be important. Regarding the remaining three trap sites, the qualitative trends are the same in that the uranium vacancy is predicted to the most stable incorporation site. However, as with our GGA calculations, the incorporation energy for Cs is positive due to the incorrect treatment of Coulombic effects.

Recently, Brillant *et al* [17, 20, 21] used the SP-GGA + U formalism and a 96-atom supercell to examine the solution of Ba, Zr and Cs in UO_2. Thus, these can be compared quantitatively with our results for Cs and a qualitative comparison can be done for Ba and Sr since both are 2+ charged defects. For Cs, both calculations predict the uranium vacancy trap site to be the most stable incorporation site followed by the divacancy. Our calculations predict the solution of Cs to be energetically favorable for the stoichiometric case, in contrast to the results of

Gupta *et al* [21]. The solution energy trend is the same when comparing Sr and Ba for all the three stoichiometries considered, although the solution of Sr is easier. This is due to the smaller size of the Sr^{2+} ion as compared to the Ba^{2+} ion.

5. Conclusions

The aim of this work was to predict the stability of selected fission products and their respective oxides in $UO_{2\pm x}$. The most stable solution site was found to depend on stoichiometry, the particular fission product and the exchange correlation functional used. Regarding our SP-GGA + U calculations, for Xe, the most stable solution site was the bound Schottky for UO_{2-x} and UO_2 and the uranium vacancy for UO_{2+x}. For Cs, the preferred solution site was the bound Schottky for UO_{2-x}, the divacancy trap site for UO_2 and the uranium vacancy for UO_{2+x} corresponding to the progressive difficulty of oxygen vacancy formation. For Sr, the energetically favorable solution site was the divacancy for UO_{2-x} and the uranium vacancy for UO_2 and UO_{2+x}. In general, higher charged defects were observed to be more soluble for all the three stoichiometries and based on this, the behavior of other fission products can be predicted.

There were differences in the GGA and SP-GGA + U methods for the solid fission products with regard to the most stable site. This was attributed to the limitation of GGA to capture the Coulombic effects completely in these charged fission products. We were also able to identify the scenarios where simplified expressions of trap formation energy could be used and where more complicated relations were required.

The solution energy model was then extended to include the binary oxides SrO and Cs_2O. Here it was possible to make favorable comparisons with experimentally observed phenomena. We were able to show the increase in solubility of the fission products with stoichiometry consistent with previous theoretical studies and experimental observations. These studies can be extended to include other fission products and microstructural features such as grain boundaries and can lead to a fundamental understanding of nuclear fuel phenomena.

Acknowledgments

PVN, SRP and SBS are happy to acknowledge support for this work through DOE-NERI Award DE-FC07-05ID14649 and the DOE-BES Computational Materials Science Network. They further acknowledge the University of Florida High-Performance Computing Center for providing computational resources and support that have contributed significantly to the research results reported here. PVN would also like to acknowledge funding from the DOE-Advanced Fuel Cycle Initiative. X-YL and BPU acknowledge the Los Alamos National Laboratory Directed Research and Development Program. LANL is operated by Los Alamos National Security, LLC, for the National Nuclear Security Administration of the US Department of Energy under Contract No. DE-AC52-06NA25396.

References

[1] Olander D R 1985 *Fundamental Aspects of Nuclear Reactor Fuel Elements* (Springfield, VA: National Technical Information Services)
[2] Ewart F T, Taylor R G, Horspool J M and James G 1976 *J. Nucl. Mater.* **61** 254
[3] Shultis J K and Faw R E 2002 *Fundamentals of Nuclear Science and Engineering* (New York: Dekker)
[4] Olander D R and Van Uffelen P 2001 *J. Nucl. Mater.* **288** 137
[5] Kleykamp H 1985 *J. Nucl. Mater.* **131** 221
[6] Oboyle D R, Brown F L and Sanecki J E 1969 *J. Nucl. Mater.* **29** 27
[7] Matzke H and Blank H 1989 *J. Nucl. Mater.* **166** 120
[8] Adamson M G and Vaidyanathan S 1981 *Trans. Am. Nucl. Soc.* **38** 289
[9] Kleykamp H 1993 *J. Nucl. Mater.* **206** 82
[10] Sari C, Benedict U and Blank H 1968 *Thermo. Nucl. Mater. Proc. Symp.* vol 3 p 587
[11] Grimes R W and Catlow C R A 1991 *Phil. Trans. R. Soc.* A **335** 609
[12] Grimes R W and Catlow C R A 1990 *J. Am. Ceram. Soc.* **73** 3251
[13] Crocombette J-P 2002 *J. Nucl. Mater.* **305** 29
[14] Freyss M, Vergnet N and Petit T 2006 *J. Nucl. Mater.* **352** 144
[15] Petit T, Freyss M, Garcia P, Martin P, Ripert M, Crocombette J P and Jollet F 2003 *J. Nucl. Mater.* **320** 133
[16] Petit T, Jomard G, Lemaignan C, Bigot B and Pasturel A 1999 *J. Nucl. Mater.* **275** 119
[17] Gupta F, Brillant G and Pasturel A 2007 *Phil. Mag.* B **87** 2561
[18] Iwasawa M, Chen Y, Kaneta Y, Ohnuma T, Geng H Y and Kinoshita M 2006 *Mater. Trans.* **47** 2651
[19] Nerikar P, Watanabe T, Tulenko J, Phillpot S and Sinnott S 2009 *J. Nucl. Mater.* **384** 61
[20] Brilliant G and Pasturel A 2008 *Phys. Rev.* B **77** 184110
[21] Gupta F, Pasturel A and Brillant G 2009 *J. Nucl. Mater.* **385** 368
[22] Baer Y and Schoenes J 1980 *Solid State Commun.* **33** 885
[23] Blochl P E 1994 *Phys. Rev.* B **50** 17953
[24] Kresse G and Joubert D 1999 *Phys. Rev.* B **59** 1758
[25] Dudarev S L, Manh D N and Sutton A P 1997 *Phil. Mag.* B **75** 613
[26] Kresse G and Furthmüller J 1996 *Phys. Rev.* B **54** 11169
[27] Kresse G and Hafner J 1993 *Phys. Rev.* B **47** 558
[28] Monkhorst H J and Pack J D 1976 *Phys. Rev.* B **13** 5188
[29] Matzke H 1987 *J. Chem. Soc. Faraday Trans.* II **83** 1121
[30] Lidiard A B 1966 *J. Nucl. Mater.* **19** 106
[31] Geng H Y, Chen Y, Kaneta Y, Iwasawa M, Ohnuma T and Kinoshita M 2008 *Phys. Rev.* B **77** 104120
[32] Geng H Y, Chen Y, Kaneta Y and Kinoshita M 2008 *Phys. Rev.* B **77** ,
[33] Geng H Y, Chen Y, Kaneta Y and Kinoshita M 2008 *Appl. Phys. Lett.* **93** 201903
[34] Andersson D A, Lezama J, Uberuaga B P, Deo C and Conradson S D 2009 *Phys. Rev.* B **79** 024110
[35] Govers K, Lemehov S, Hou M and Verwerft M 2007 *J. Nucl. Mater.* **366** 161
[36] Gale J 1997 *J. Chem. Soc. Faraday Trans.* **93** 629
[37] Gale J D and Rohl A L 2003 *Mol. Simulat.* **29** 291
[38] Larson P and Lambrecht W R L 2007 *Phys. Rev.* B **75** 045114
[39] Amadon B, Jollet F and Torrent M 2008 *Phys. Rev.* B **77** 155104
[40] Thomas L E, Beyer C E and Charlot L A 1992 *J. Nucl. Mater.* **188** 80